Canadian Mineralogist
Vol. 15, pp. 50-58 (1977)

REFINEMENT OF THE CRYSTAL STRUCTURE OF $LiScSi_2O_6$ AND STRUCTURAL VARIATIONS IN ALKALI PYROXENES

F. C. HAWTHORNE* AND H. D. GRUNDY
Department of Geology, McMaster University, Hamilton, Ontario

ABSTRACT

The crystal structure of $LiScSi_2O_6$ — *a* 9.8033(7), *b* 8.9581(7), *c* 5.3515(4)Å, β 110.281(4)°, *C*2/*c* — has been refined to an *R* index of 2.4% for 799 observed reflections. The structure is similar to that of spodumene ($LiAlSi_2O_6$), but the tetrahedral chain element is in an *O*-rotated configuration in $LiScSi_2O_6$ whereas it assumes an *S*-rotated configuration in spodumene. The geometrical changes in the alkali pyroxenes are discussed as functions of site chemistry.

SOMMAIRE

La structure cristalline de $LiScSi_2O_6$ — *a* 9.8033(7), *b* 8.9581(7), *c* 5.3515(4)Å, β 110.281(4)°, *C*2/*c* — est affinée jusqu'à un résidu de 2.4% pour 799 réflexions observées. La structure ressemble à celle du spodumène ($LiAlSi_2O_6$), mais le maillon de la chaîne tétraédrique est en configuration rotation *O* dans $LiScSi_2O_6$, tandis qu'il présente une configuration rotation *S* dans le spodumène. Les changements géométriques observés dans les pyroxènes alcalins sont fonctions de la chimie de site.

(Traduit par la Rédaction)

INTRODUCTION

The pyroxene structure is one of extreme chemical compliance and will accept a wide variety of cations in the *M* (and tetrahedral) sites. Because of this, structural changes may be studied in great detail over a variety of chemistries that are not represented in the naturally occurring minerals. The alkali-metal pyroxenes are extremely attractive in this respect; compositions of the form $M^+M^{3+}Si_2O_6$ will accept trivalent cations from Al ($r = 0.535$Å) to In ($r = 0.80$Å), a very large variation in cation size that encompasses both closed- and open-shell cations. The effect of tetrahedral substitutions may also be examined by comparison with homotypic germanates, and metavanadates and meta-arsenates of the form $M^+X^{5+}O_3$.

The structure of jadeite was refined by Prewitt & Burnham (1966); refinements of spodumene, $LiFe^{3+}Si_2O_6$, ureyite, acmite, $NaInSi_2O_6$ and $NaScSi_2O_6$ have been presented by Clark *et al.* (1969), Christensen & Hazell (1967) and Hawthorne & Grundy (1973, 1974). The structure of $LiScSi_2O_6$ has been refined here in order to facilitate a comparison of structural variations in the Li and Na pyroxenes.

EXPERIMENTAL

The crystals used in this investigation were synthesized by Dr. Jun Ito of Harvard University; details of the method of synthesis and physical properties are given by Ito & Frondel (1968). Precession photographs exhibited monoclinic symmetry with systematic absences consistent with the space group *C*2/*c*. Exposure times of up to 300 hours showed no reflections violating either the *c* glide-plane criterion, as was found with $LiAlSi_2O_6$ (Appleman & Stewart 1966; Clark *et al.* 1969) and $LiFeSi_2O_6$ (Clark *et al.* 1969) or the *C*-centring criterion, as was found with $LiAlGe_2O_6$ and $LiGaGe_2O_6$ (Hahn & Behruzi 1968). Numerous crystals were examined by the precession method and all were twinned with (100) as the twin plane; the crystal showing the least amount of twinning was chosen for the collection of intensities. Cell dimensions were determined by least-squares refinement of 15 reflections automatically aligned on a 4-circle diffractometer (Table 1).

A cleavage fragment 0.14×0.05×0.07 mm

TABLE 1. MISCELLANEOUS INFORMATION

a	9.8033(7)Å	crystal	0.14x0.07
b	8.9581(7)	dimensions	x0.05 mm
c	5.3515(4)	no. of $\|F_{obs}\|$	940
β	110.281(4)°	no. of $\|F_{obs}\| > 4\sigma$	799
V	440.83	R (obs.)	2.4%
z	4	R (all data)	3.2%
Space Group	C2/c	R_w (obs.)	2.8%
μ(cm^{-1})	21.7	R_w (all data)	3.7%

$$R = \sum(|F_{obs}| - |F_{calc}|)/\sum|F_{obs}|$$

$$R_w = (\sum w(|F_{obs}| - |F_{calc}|)^2/\sum wF_{obs}^2)^{\frac{1}{2}},\ w = 1$$

Temp. factor form used: $\exp(-\sum_{i=1}^{3}\sum_{j=1}^{3} h_i h_j \beta_{ij})$

*Present address: Department of Earth Sciences, University of Manitoba, Winnipeg, Manitoba R3T 2N2.

was used to collect the intensity data using Mo$K\alpha$ radiation and a Syntex $P\bar{1}$ automatic diffractometer according to the experimental procedure of Hawthorne & Ferguson (1975). A total of 940 reflections was collected over one asymmetric unit out to a value of 65°2θ. The data were corrected for absorption (for polyhedral crystal shape), Lorentz, polarization and background effects, and subsequently reduced to structure factors. A reflection was considered as observed if its magnitude exceeded that of four standard deviations based on counting statistics. This resulted in 940 unique reflections of which 799 were classed as observed.

Refinement

As a consequence of the twinning, reflections of the type $hk0$ overlap with equivalent reflections of the type $hk0$ from the corresponding twinned part of the crystal; for $l \neq 0$, there is no overlap. Consequently, the data were divided into two sets (one with $l=0$ and the other with $l \neq 0$) with separate scale factors. Scattering factors for O^{-1} and fully ionized cations were taken from Cromer & Mann (1968) and coefficients for anomalous dispersion were taken from Cromer (1965). The final atomic coordinates and equivalent isotropic temperature factors for $LiFe^{3+}Si_2O_6$ (Clark *et al.* 1969) were used as input parameters to the least-squares program RFINE (Finger 1969). After several cycles of least-squares refinement, gradually increasing the number of variables, the structure converged at a conventional R of 3.2%. The temperature factors were then converted to anisotropic of the form given in Table 1 and a correction was made for isotropic extinction with the extinction coefficient being included as a variable in the refinement (Zachariasen 1968). Further cycles of refinement resulted in convergence at conventional R of 2.4% (observed reflections) and 3.2% (all reflections) and weighted R_w (unit weights) of 2.8% (observed reflections) and 3.7% (all reflections).[1] Comparison of the final scale factors indicated a twin ratio of 1:0•022. Final positional parameters and anisotropic temperature factor coefficients are presented in Tables 2 and 3. Interatomic distances and angles were calculated with the program ERRORS (L. W. Finger, pers. comm.) and are presented in Tables 4 and 5 respectively. The magnitudes and orientations of the principal axes of the thermal ellipsoids were calculated with the program ERRORS and are given in Table 6.

[1]Structure factor tables are available, at a nominal charge, from the Depository of Unpublished Data, CISTI, National Research Council of Canada, Ottawa, Canada, K1A 0S2.

TABLE 2. ATOMIC PARAMETERS FOR $LiScSi_2O_6$

Atom	x	y	z	B_{equiv}
O1A1	0.1209(1)	0.0835(1)	0.1582(3)	0.46(2)
O2A1	0.3709(2)	0.2486(3)	0.3448(3)	0.71(2)
O3A1	0.3545(2)	0.0057(2)	0.0579(3)	0.83(2)
SiA1	0.29900(5)	0.08678(5)	0.2778(1)	0.40(1)
M1	0	0.89501(5)	1/4	0.40(1)
M2	0	0.2574(7)	1/4	1.54(9)

TABLE 3. ANISOTROPIC TEMPERATURE FACTOR COEFFICIENTS*

	β_{11}	β_{22}	β_{33}	β_{12}	β_{13}	β_{23}
O1A1	101(11)	183(13)	451(38)	-11(9)	70(16)	11(17)
O2A1	221(13)	180(13)	893(48)	-76(10)	222(21)	-83(19)
O3A1	161(13)	400(15)	661(49)	-46(11)	116(20)	-278(20)
SiA1	112(4)	145(5)	363(16)	-19(4)	072(6)	-4(6)
M1	126(4)	129(4)	376(15)	0	081(6)	0
M2	536(68)	593(72)	962(196)	0	311(94)	0

*$\beta_{ij} \times 10^5$

TABLE 4. SELECTED INTERATOMIC DISTANCES

Si Tetrahedron		M1 Octahedron	
SiA1-O1A1	1.638(3)	M1-O1A1, B1	2.214(2)
SiA1-O2A1	1.598(2)	M1-O1A2, B2	2.102(5)
SiA1-O3A1	1.628(2)	M1-O2C1, D1	2.006(2)
SiA1-O3A2	1.632(3)	Mean	2.107
Mean	1.624	O1A1-O1B1	2.863(4)
O1A1-O2A1	2.738(4)	O2C1-O2D1	3.036(4)
O1A1-O3A1	2.621(3)	O1A1-O2C1	3.109(2)
O1A1-O3A2	2.657(7)	O1A1-O1A2	3.066(1)
O2A1-O3A1	2.636(2)	O1A2-O2C1	3.001(2)
O2A1-O3A2	2.578(2)	O1A2-O2D1	2.869(6)
O3A1-O3A2	2.678(1)	O1A1-O1B2	2.818(6)
Mean	2.651	Mean	2.969
M2 Antiprism		**Cation-Cation**	
M2-O1A1	2.116(5)	Si-SiA2	3.095(1)
M2-O2C2	2.099(6)	M1-M1(1)	3.271(1)
M2-O3C1	2.651(6)	M1-SiA1	3.356(1)
M2-O3C2	3.299(5)	M1-SiA2	3.295(1)
Mean [6]	2.289		
Mean [8]	2.541		

TABLE 5. SELECTED INTERATOMIC ANGLES FOR $LiScSi_2O_6$

Si Tetrahedron		M1 Octahedron		Chain Angles	
O1A1-Si-O2A1	115.6(1)	O1A1-M1-O1B1	80.6(1)	SiA1-O3A1-SiA2	143.3(1)
O1A1-Si-O3A1	106.7(2)	O1A1-M1-O2C1	90.5(1) x2	O3A2-O3A1-O3A2	175.6(1)
O1A1-Si-O3A2	108.7(2)	O1A1-M1-O1A2	90.5(1) x2	SiA1-O1A1-M1	120.5(1)
O2A1-Si-O3A1	109.6(1)	O1A1-M1-O1B2	81.5(1) x2	SiA2-O1A2-M1	123.0(2)
O2A1-Si-O3A2	105.9(1)	O1A2-M1-O2C1	98.3(1) x2	SiC1-O2C1-M1	143.6(1)
O3A1-Si-O3A2	110.4(1)	O1A2-M1-O2D1	88.6(1) x2	SiA1-O1A1-M2	120.2(1)
Mean	109.5	O2C1-M1-O2D1	98.6(1)	SiC2-O2C2-M2	90.3(2)
		Mean	89.8		

Discussion

The basic structure of the pyroxenes has been adequately described by Prewitt & Burnham (1966), Zussman (1968), and a detailed consideration of pyroxene topologies is given by Papike *et al.* (1973). The structure is shown in Figure 1 which adheres to the site nomenclature proposed by Burnham *et al.* (1967). Ionic radii used in the following discussion are from Shannon & Prewitt (1969, 1970).

The variation in structural parameters across the lithium pyroxene series is strongly dependent on the ionic radius of the *M*1 cation. Figure 2 shows the variation in the mean cation-anion distances with the ionic radius of the *M*1 cation; a marked positive linear correlation is observed in each case. The octahedra of the *M*1 chain are edge-sharing and consequently form a much more rigid unit than the corner-sharing tetrahedra of the silicate chain. Thus the various distortions in the pyroxenes are partly the result of the articulation requirements between these two basic units. The variation in the *c*-dimension is controlled largely by the *M*1 cation radius in the alkali pyroxenes (except for $NaInSi_2O_6$ where additional constraints occur); the type of alkali cation occupying the *M*2 site has only minor influence (Table 7). In addition, distortions are also imposed by the coordination requirements of the *M*2 cation. Lithium is six-coordinate but sodium is eight-coordinate (Clark *et al.* 1969). This coordination-number change is effected by a relative displacement of the 'back-to-back' tetrahedral chains in the *c* direction. The separation of the mid-points of the O3-O3 tetrahedral edges projected onto the *b-c* plane provides a measure of this chain displacement. Chain displacements for the monoclinic pyroxenes are shown in Table 8. They fall into three groups, corresponding to the *M*2 site occupancy and, as such, reflect the major changes in the value of the β angle. The calcic pyroxenes with the smallest chain-displacements have the more regular *M*2 site; the sodic pyroxenes exhibit greater chain-displacements with the concomitant larger distortions of the *M*2 site. The lithium pyroxenes show by far the largest chain-displacements which cause the change in *M*2 coordination number from [8] to [6]. This is illustrated in Figure 3 where the variation in *M*2 distortion[1] with chain-displacement is shown; this effect is compounded if the size of the *M*1 cation is increased due to an expansion of the octahedral chain. The extreme distortions exhibited by the *M*2 site in the Li pyroxenes (when considered as eight-coordinate) indicate the coordination number change from eight to six.

As the back-to-back tetrahedral chains link in the *b*-direction to the octahedral chains via the O2-O2 edge of the *M*1 octahedron, the relative displacement of the O2 atoms in the *c*-direction is an important factor in controlling the tetrahedral chain displacement. Superimposed

TABLE 6. ELLIPSOIDS OF VIBRATION IN $LiScSi_2O_6$

	R.M.S. Displacement	Angle to a-axis	Angle to b-axis	Angle to c-axis
O1A1	0.065(4) Å	16(10)°	81(7)°	97(14)°
	0.076(3)	79(14)	78(12)	167(12)
	0.087(3)	101(7)	15(11)	76(12)
O2A1	0.071(4)	52(6)	38(5)	96(6)
	0.093(3)	49(6)	115(6)	144(6)
	0.115(3)	64(5)	117(4)	55(6)
O3A1	0.070(4)	88(13)	61(2)	36(8)
	0.083(3)	178(10)	88(7)	69(11)
	0.141(2)	88(2)	29(2)	118(2)
SiA1	0.066(1)	28(5)	62(5)	114(25)
	0.068(1)	93(22)	97(12)	156(24)
	0.080(1)	118(4)	28(4)	85(5)
M1	0.069(1)	112(11)	90	2(11)
	0.072(1)	90	0	90
	0.073(1)	22(11)	90	88(11)
M2	0.106(12)	107(10)	90	4(10)
	0.152(9)	163(10)	90	86(10)
	0.155(9)	90	0	90

[1]Distortion $\delta = \sum_{i=1}^{n} [(l_i - l_o)/l_o]^2/n$, where l_o = mean bond length and l_i = individual bond lengths.

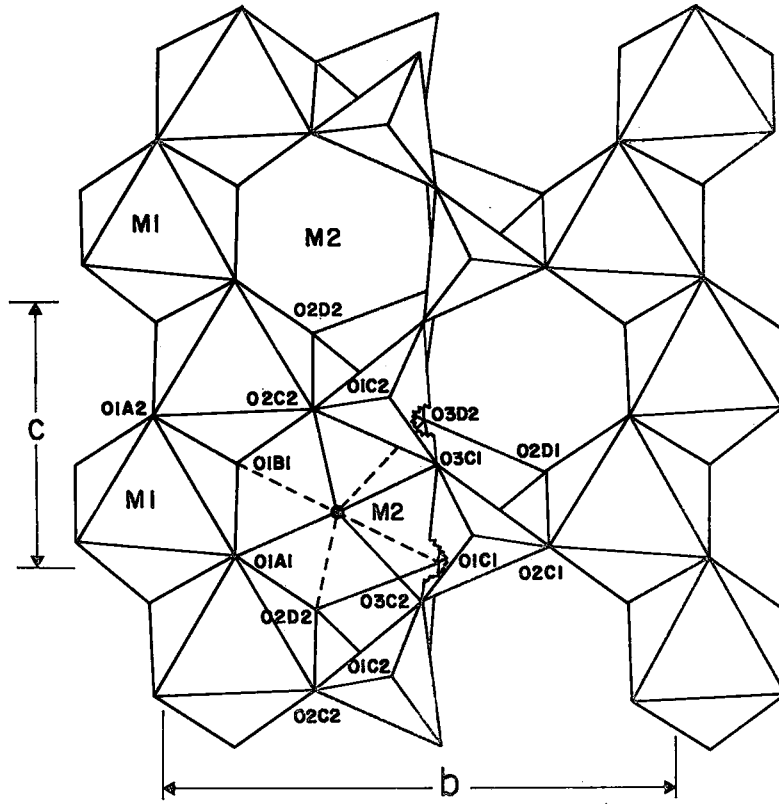

FIG. 1. a^* axis projection of the clinopyroxene structure.

upon this is the mechanism of *O*-rotation (Thompson 1970; Papike *et al.* 1973) which decreases the amount of tetrahedral chain displacement. These parameters are given in Table 8 for the $C2/c$ pyroxenes. The O2-O2 displacement is primarily controlled by *M*2-O2 interaction, as the O2 anion is formally underbonded (Shannon & Calvo 1973) and requires very short anion-cation distances. The relative variation in *M*2-O2 as the ionic radius of the *M*1 cation increases is consistent in the Li and the Na pyroxenes. When *M*1=Al, *M*2-O2 is the longest *M*2-O bond length, when *M*1=Fe it is intermediate and when *M*1=Sc it is the shortest bond length. This seems to be the result of the articulation constraints between the octahedral and tetrahedral chains. When a small cation occupies *M*1, the octahedral chain is undersized with respect to the tetrahedral chain. Thus the cation-cation repulsion across the O1-O1 shared edge of the *M*1 chain produces a large displacement of the cations away from each other, extending the octahedral chain and promoting inter-chain linkage. This also results in an increase in the *M*1-O1 bond lengths and a decrease in the *M*1-O2 bond lengths, and thus *M*2-O1 is considerably shorter than *M*2-O2. As the size of the *M*1 cation increases, this effect is gradually reduced as the octahedral chain becomes larger and the tetrahedral chain begins to exert a constraining effect on *c*-axis expansion, reducing the amount of cation repulsion relaxation and decreasing the relative difference between *M*1-O1 and *M*1-02. Thus the relative bond strength requirements of O1 and O2 change with *M*2-O1 lengthening and *M*2-O2 shortening relative to each other. Hence with *M*1=Sc, the amount of cation repulsion relaxation is small and *M*2-O2 is shorter than *M*2-O1. It is rather interesting to examine $NaCr^{3+}Si_2O_6$ in the light of this proposed mechanism. This pyroxene shows a very short *M*1-*M*1 distance that has been taken to indicate weak metal-metal bonding across the shared edge of the *M*1 octahedra (Hawthorne & Grundy 1973). The mechanism suggested above would indicate that this pyroxene should show an anomalously short *M*2-O2 bond length, and in fact $NaCr^{3+}Si_2O_6$ exhibits the shortest *M*2-O2 bond length of any of the sodic pyroxenes examined so far. This relative change in the *M*2-O2 bond length with increasing *M*1 cation radius is accomplished by a rotation and expansion of the O2-O2 edge of the *M*1 octahedron. This rotation and extension of O2-O2 increases the *c*-axis separation of the

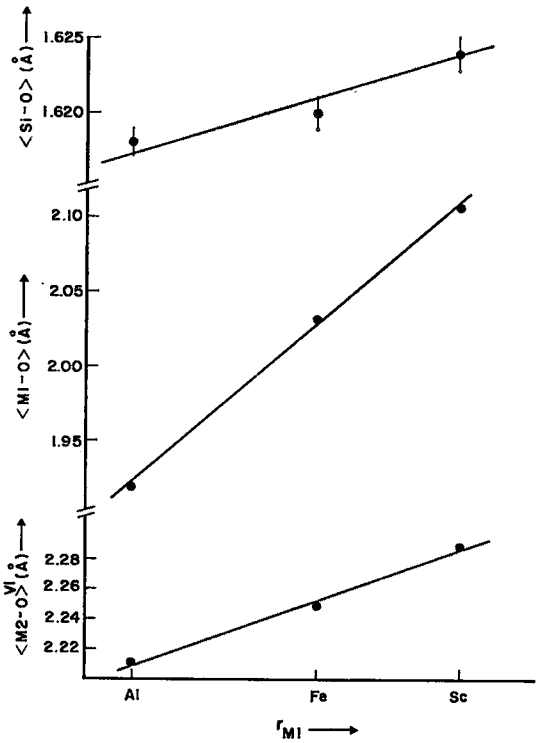

FIG. 2. Variation in mean cation-oxygen distances with the ionic radius of the *M*1 cation for the Li pyroxenes.

symmetry-related O2 anions, leading to an increase in the tetrahedral chain displacement.

Also contributing to the tetrahedral chain displacement is the amount of *O*-rotation of the tetrahedral chains. This effect may be envisaged as being superimposed on the effect of the O2-O2 displacement to produce the chain displacement required by the *M*2 cation. Figure 4 shows the variation in *O*-rotation with *M*1 cation radius for the alkali pyroxenes. The Li pyroxenes show a much greater range of rotation which exhibits a positive correlation with the radius of the cation of the *M*1 site. The Na pyroxenes show a much smaller range; however, $NaInSi_2O_6$ shows a much larger *O*-rotation than the other Na pyroxenes and the slope of the graph between $NaScSi_2O_6$ and $NaInSi_2O_6$ becomes sub-parallel to the trend in the Li pyroxenes. This correlates with the variation in *M*2-O2 across each pyroxene series. In the Li pyroxenes, *M*2-O2 decreases with increasing *M*1 cation size; in the Na pyroxene, *M*2-O2 is constant across the series to $NaInSi_2O_6$, where *M*2-O2 decreases. The variation in O-rotation with O2-O2 displacement for the alkali pyroxenes is shown in Figure 5. It is apparent that the mechanisms of O2-O2 displacement and O-rotation act in a complementary manner to produce the tetrahedral chain displacement required by the structure (Table 8).

It is of considerable interest to examine how the linkage is maintained between the tetrahedral and octahedral chains as the ionic radius of the *M*1 cation increases, as this can be seen as exerting a limiting effect on possible pyroxene compositions. From *M*1 = Al to Sc, the octahedral chain expands linearly in the *c*-direction for both the Li and Na pyroxenes. However, the way in which the tetrahedral chain expands differs with the *M*2 occupancy. In the Li pyroxenes, the O3-O3 tetrahedral edge expands and

TABLE 7. CELL DIMENSIONS FOR THE LITHIUM PYROXENES AND THEIR SODIUM ANALOGUES

	a (Å)	b (Å)	c (Å)	β (°)	a sinβ (Å)
$LiAlSi_2O_6$ [1]	9.449	8.386	5.215	110.10	8.874
$NaAlSi_2O_6$ [2]	9.418	8.562	5.219	107.58	8.978
$LiFeSi_2O_6$ [1]	9.666	8.669	5.294	110.15	9.074
$NaFeSi_2O_6$ [1]	9.658	8.795	5.294	107.42	9.215
$LiScSi_2O_6$ [3]	9.803	8.958	5.352	110.28	9.196
$NaScSi_2O_6$ [4]	9.844	9.044	5.354	107.22	9.403

[1] Clark et al. (1969). [2] Prewitt & Burnham (1966). [3] This study. [4] Hawthorne & Grundy (1973).

TABLE 8. VARIATION IN DISTORTIONAL PARAMETERS IN THE C2/c PYROXENES

	1 (Å)	2 (Å)	3 (°)	4 (°)	5 (°)
$LiAlSi_2O_6$	1.535	1.410	4.8	-9.5	1.8
$LiFeSi_2O_6$	1.531	1.721	-0.3	0.0	2.6
$LiScSi_2O_6$	1.609	1.892	-3.3	4.4	3.9
$NaAlSi_2O_6$	0.895	1.240	8.9	5.3	1.7
$NaCrSi_2O_6$	0.911	1.368	7.1	7.9	1.6
$NaFeSi_2O_6$	0.982	1.350	8.0	6.0	1.5
$NaScSi_2O_6$	1.063	1.433	6.9	6.4	2.1
$NaInSi_2O_6$	1.075	1.571	5.0	9.2	2.0
$CaMgSi_2O_6$	0.736	1.444	6.3	13.6	2.6
$CaFeSi_2O_6$	0.822	1.452	6.2	15.5	3.1
$CaMnSi_2O_6$	0.763	1.570	4.4	16.2	3.7

1 -- Back-to-back tetrahedral chain displacement
2 -- O(2)-O(2) displacement along c
3 -- O(2)-O(2) shear
4 -- Tetrahedral O-rotation
5 -- c-axis tetrahedral rotation

the O3-Si-O3 angle increases, thus increasing the chain length without greatly increasing the <Si-O(br)> distance. In the Na pyroxenes, from $M1$ = Al to Sc the tetrahedral chain expands by an increase in the <Si-O(br)> distance (Fig. 6); for $NaInSi_2O_6$ there is no furthter increase in Si-O(br) or significant increase in the length of the octahedral chain. Presumably the tetrahedral

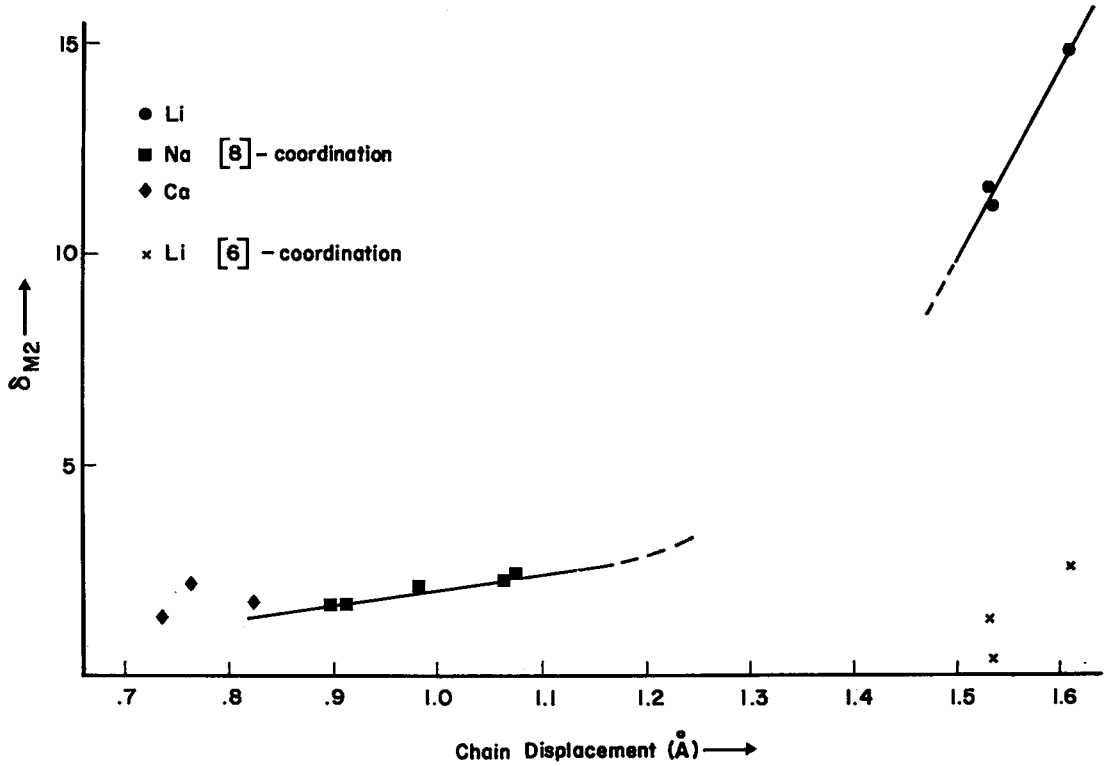

FIG. 3. $M2$ bond length distortion versus tetrahedral chain-displacement for the ordered clinopyroxenes.

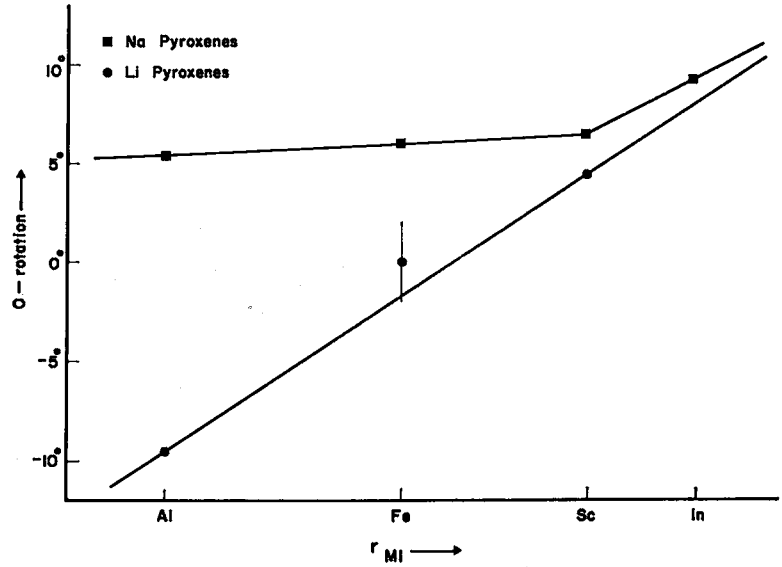

FIG. 4. Variation in O-rotation with ionic radius of the $M1$ cation for the ordered alkali pyroxenes.

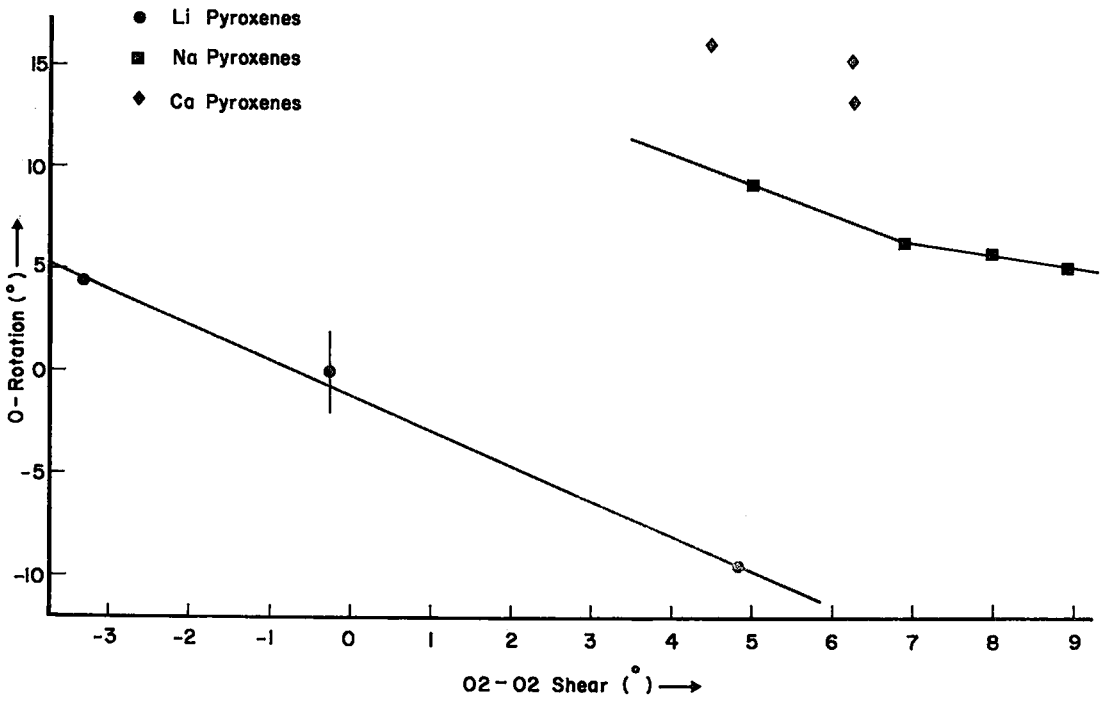

FIG. 5. Variation in *O*-rotation with O2-O2 shear for the ordered clinopyroxenes.

chain has expanded as far as it can for *M*2=Na and is exerting a constraining effect on the *c*-axis expansion of the octahedral chain.

As the *M*1 cation radius increases, the *M*1 octahedron also expands in the *b*-direction. This may be accommodated by the tetrahedral chain in two ways:

(1) rotation of the tetrahedra round an axis through the midpoints of the O3-O3 edges (*c*-axis rotation). An anticlockwise rotation (when viewed along *c*) of the SiAl tetrahedron is defined as positive, with the rotation defined as the angular deviation of O2*A*1 from the plane parallel to *b*-*c* through O3*A*1 and O3*A*2. This is illustrated in Figure 7.

(2) Distortion of tetrahedral edges leading to an increase in *b*-axis separation of glide-related O1 anions. Table 8 gives the *c*-axis rotations for the *C*2/*c* pyroxenes. For the Li pyroxenes, octahedral *b*-axis expansion is accommodated by *c*-axis rotation of the tetrahedral chain. For the Na pyroxenes, the more important mechanism of accommodation is by tetrahedral edge distortion. This is shown by Figure 8 which shows the variation in selected tetrahedral edge lengths with *M*1 cation radius for the Na pyroxenes. Decrease in O1*A*1-O2*A*1 and increase in O1*A*1-O3*A*1 and O1*A*1-O3*A*2 produce an increase in the *b*-axis separation of the *c*-glide related O1 atoms. Note that this mechanism is not as prominent between *M*1=Fe and *M*1=Sc since an increase in *c*-axis rotation of the tetrahedron occurs in this range (Table 7). It is interesting to note that *c*-axis tetrahedral rotation will affect the Si-O3-Si angle whereas tetrahedral edge

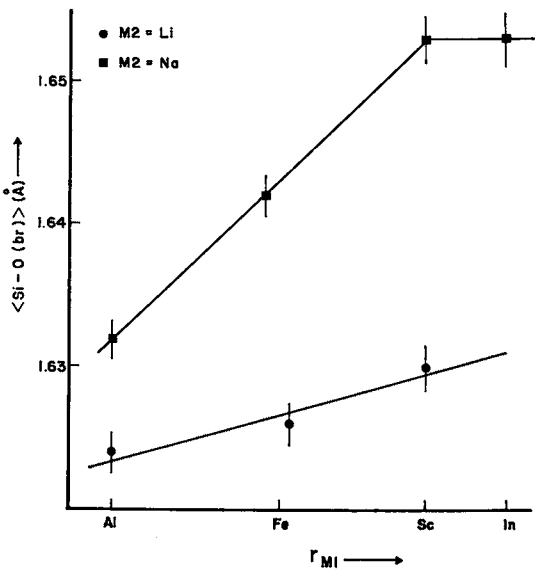

FIG. 6. Variation in mean Si-O(br) bond length with ionic radius of the *M*1 cation for the alkali pyroxenes.

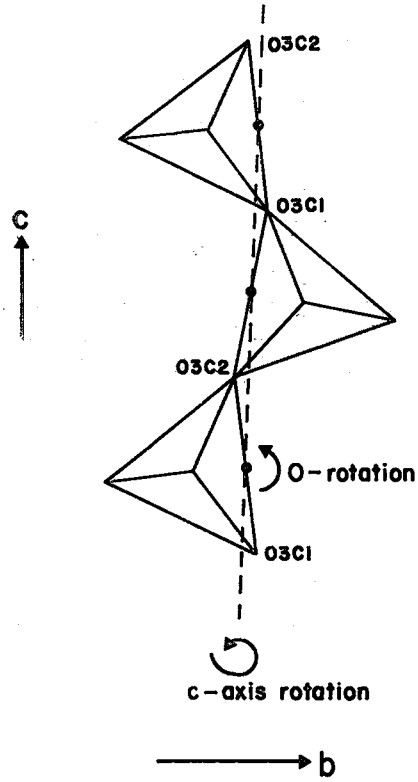

FIG. 7. Part of the tetrahedral chain, showing the various rotations used to describe the chain distortions.

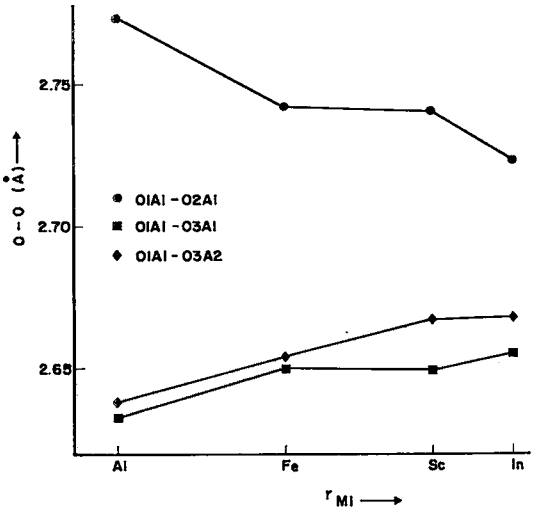

FIG. 8. Variation in selected tetrahedral edge lengths with the ionic radius of the *M*1 cation for the sodic pyroxenes.

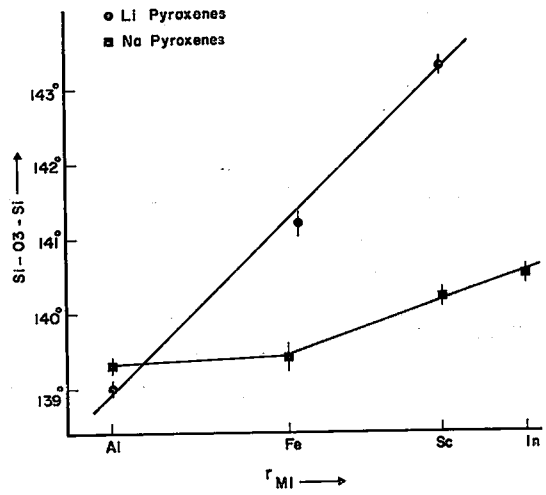

FIG. 9. Variation in chain angle Si-O3-Si with the ionic radius of the *M*1 cation for the alkali pyroxenes.

length distortion does not necessarily do so. This leads to a difference in behavior in Si-O3-Si with increasing *M*1 cation radius (and increasing Si-O(br) bond lengths) in the two pyroxene series. This is shown in Figure 9, which indicates that the Si-O3-Si angle is responsive to the mechanism of *b*-axis expansion.

ACKNOWLEDGEMENTS

H. D. Grundy would like to acknowledge a grant from the National Research Council of Canada which supported this work. The authors would like to thank Dr. Jun Ito, University of Chicago, for supplying the crystals used in this study.

REFERENCES

APPLEMAN, D. E. & STEWART, D. B. (1966): Crystal chemistry of spodumene type pyroxenes. *Geol. Soc. Amer., Progr. Ann. Meet. San Francisco, California*, 5-6.

CAMERON, M., SUENO, S., PREWITT, C. T. & PAPIKE, J. J. (1973): High-temperature crystal chemistry of acmite, diopside, hedenbergite, jadeite, spodumene, and ureyite. *Amer. Mineral.* 58, 594-618.

CHRISTENSEN, A. N. & HAZELL, R. G. (1967): The crystal structure of $NaIn(SiO_3)_2$. *Acta Chem. Scand.* 21, 1425-1429.

CLARK, J. R., APPLEMAN, D. E. & PAPIKE, J. J. (1969): Crystal-chemical characterization of clinopyroxenes based on eight new structure refinements. *Mineral. Soc. Amer. Spec. Pap.* 2, 31-50.

CROMER, D. T. (1965): Anomalous dispersion corrections computed from self-consistent field relativistic Dirac-Slater wave functions. *Acta Cryst.* 18, 17-23.

——— & MANN, J. B. (1968): X-ray scattering factors computed from numerical Hartree-Fock wave functions. *Acta Cryst.* 24, 321-324.

FINGER, L. W. (1969): RFINE. A Fortran IV computer program for structure factor calculation and least-squares refinement of crystal structures. *Geophy. Lab., Carnegie Inst. Wash.* (unpublished manuscript).

HAHN, T. & BEHRUZI, M. (1958): New germanates with chain structures. *Z. Krist.* 127, 160-163.

HAWTHORNE, F. C. & FERGUSON, R. B. (1975): Refinement of the crystal structure of cryolite. *Can. Mineral.* 13, 277-382.

——— & GRUNDY, H. D. (1973): Refinement of the crystal structure of $NaScSi_2O_6$. *Acta Cryst.* B29, 2615-2616.

——— & ——— (1974): Refinement of the crystal structure of $NaInSi_2O_6$. *Acta Cryst.* B30, 1882-1884.

ITO, J. & FRONDEL, C. (1968): Syntheses of the scandium analogues of aegirine, spodumene, andradite and melanotekite. *Amer. Mineral.* 53, 1276-1280.

PAPIKE, J. J., PREWITT, C. T., SUENO, S. & CAMERON, M. (1973): Pyroxenes: comparisons of real and ideal structural topologies. *Z. Krist.* 136, 254-273.

——— & ROSS, M. (1970): Gedrites: crystal structures and intracrystalline cation distributions. *Amer. Mineral.* 55, 1945-1972.

PREWITT, C. T. & BURNHAM, C. W. (1966): The crystal structure of jadeite, $NaAlSi_2O_6$. *Amer. Mineral.* 51, 956-975.

SHANNON, R. D. & CALVO, C. (1973): Crystal structure of $LiVO_3$. *Can. J. Chem.* 51, 265-273.

THOMPSON, J. B. (1970): Geometrical possibilities for amphibole structures: model biopyriboles. *Amer. Mineral.* 55, 292-293.

ZACHARIASEN, W. H. (1968): Extinction and Boorman effect in mosaic crystals. *Acta Cryst.* A24, 421-424.

ZUSSMAN, J. (1968): The crystal chemistry of pyroxenes and amphiboles. 1. Pyroxenes. *Earth Sci. Rev.* 4, 39-67.

Manuscript received June 1976, emended August 1976.